

Optimal Design of a Surface Precipitation Network in Canada

DOMINIQUE BRUNET^a AND JASON A. MILBRANDT^a

^a *Meteorological Research Division, Environment and Climate Change Canada, Toronto, Ontario, Canada*

(Manuscript received 27 May 2022, in final form 24 November 2022)

ABSTRACT: The surface precipitation network in Canada suffers from large data gaps due to the challenge of covering a large country with a low population density. A proof-of-concept for an optimal network design is proposed to more efficiently estimate precipitation in Canada with the design goal of minimizing the interpolation uncertainty. The network design is based on a statistical model of precipitation that accounts for intermittency and non-Gaussianity of precipitation. Our results indicate that the greatest needs for new stations are in British Columbia, where coastal and mountain climate leads to more uncertainty in precipitation amounts, while the Prairie Provinces (Alberta, Saskatchewan, and Manitoba) could gain efficiencies by reducing their network size. Despite the current low density of stations in the territories north of Canada, these drier and colder regions only have a moderate need for more stations, mostly in the mountainous regions of Yukon. However, from a spatially varying wind undercatch measurement error model, it is shown that these northern regions have greatest need for higher-accuracy measurements.

SIGNIFICANCE STATEMENT: The proposed methodology can guide in the optimal placement of precipitation gauges across a large country such as Canada, which will provide value for money in how rain and snow are monitored.

KEYWORDS: North America; Precipitation; Gauges; Interpolation schemes; Uncertainty; Experimental design

1. Introduction

Precipitation observations are an integral part of hydrometeorological analysis and forecast systems. Precipitation observations can either be obtained from in situ measurements or derived from remote sensing. While in situ measurements generally provide the best estimates for the ground truth, they can only provide direct information for a very localized area with a potential lack of representativity for the surrounding area. Remote sensing techniques generally offer better spatial coverage but at the cost of lower accuracy. Moreover, satellite- and radar-based quantitative precipitation estimation (QPE) techniques (see [Huffman et al. 2019](#); [Boodoo et al. 2015](#); [Zhang et al. 2016](#); [Seo 1998](#); [Seo and Breidenbach 2002](#); [Seo et al. 2014](#)) rely on surface measurements for validation and calibration. A good network of surface precipitation stations is thus an essential requirement for estimating precipitation falling within a given area of interest.


Optimal network design (OND), also called observation targeting by [Ancell and Hakim \(2007\)](#), seeks to find the best possible configuration of a network of sensors according to some network performance metric ([Chacon-Hurtado et al. 2017](#); [Mishra and Coulibaly 2009](#)). An optimal network can provide cost savings by reducing redundant measurements within a network or enhancing quality of measurements by extracting the maximal information content for each measurement given

a fixed budget. Efficient measurement of each meteorological field is particularly needed for a spatially large country like Canada, since for a given budget per capita it is not feasible to achieve the same network density as more densely populated countries.

The current network of networks for surface precipitation sensors in Canada has a variable density, with higher density in more populated areas in southern Canada and south-central Alberta, and a very low density north of 55°N. Although needs for better precipitation measurements are in part linked to population density, the global nature of meteorological processes also requires measurements even in less populated areas in order to predict weather and flooding accurately. With investments to install new sensors and financial pressures to reduce the number of sensors maintained, there is an opportunity and need to reexamine the current network design.

In this paper, we propose a new method for OND based on the minimization of the interpolation uncertainty as estimated by a spatial statistical model. Starting from the current network, modifications by addition, removal, or relocation of stations can be optimized according to the design goal of the network. As a proof-of-concept, several network design experiments are carried out over a large domain in Canada, demonstrating how small practical changes of adding or moving a few gauges can make a huge difference.

The proposed solution takes advantage of statistical modeling of precipitation to provide a quantification of uncertainty in probabilistic QPE, with minimization of the uncertainty as the network design goal. Specifically, precipitation is statistically modeled from a modification of Gaussian processes (GP) (see [Rasmussen and Williams 2006](#)) that accounts for intermittency and non-Gaussianity, while introducing an anisotropic

 Denotes content that is immediately available upon publication as open access.

Corresponding author: Dominique Brunet, dominique.brunet@ec.gc.ca

and nonstationary covariance structure estimated directly from reanalysis. GP are closely linked to kriging (see [Cressie 1990](#)), optimal interpolation (see [Gandin 1965](#); [Daley 1993](#)), and ensemble Kalman filter (see [Hamill and Snyder 2002](#)). However, instead of focusing on the deterministic estimation of the expected precipitation, the estimated variance of the interpolated precipitation is used as a measure of uncertainty. As such, the proposed OND method is more closely related to a probabilistic QPE system like the Ensemble Meteorological Dataset for North America (EMDNA) of [Tang et al. \(2021\)](#) than to a deterministic QPE system such as the Canadian Precipitation Analysis (CaPA) of [Fortin et al. \(2018\)](#). A greedy search approach is taken to select stations to add or remove. Network design experiments then compare the design of a network from a blank slate to a modification of the current network of networks by adding, removing, or moving a number of stations.

We distinguish between four possible OND goals: (i) building an OND from scratch (or blank slate), (ii) augmenting a current network by optimally adding more stations, (iii) reducing a current network by optimally removing redundant stations, and (iv) modifying a current network by selecting and relocating a number of stations. For each of these OND goals, specialized techniques have been developed. For example, [Soares et al. \(2018\)](#) applied hierarchical clustering methods to identify redundant air quality monitoring stations or to design a network using numerical model outputs for the oil sands region in northern Alberta while [Kalinić et al. \(2021\)](#) selected potential wind buoy locations over the Adriatic Sea by *K*-means clustering of model reanalysis data. Observation system experiment (OSE) or data denial experiments compare analysis or forecasts with and without a subset of observations assimilated. They are computationally expensive to run, but provide a direct estimation of the impact of a subset of observations, thus providing guidance for reducing networks. For example, in a small case study, [Seo et al. \(2015\)](#) analyzed the impact of removing rain gauges on the variance of precipitation areal average theoretically estimated from a geostatistic model fitted on radar observations. The impact of reduction of a precipitation network on hydrological forecasts was studied in particular by [Ahnert et al. \(2014\)](#).

On the other hand, observing system simulation experiments (OSSE) from [Hoffman and Atlas \(2016\)](#) go one step further than OSE by allowing the simulation of observation systems before deployment. OSSE starts with a free run (called the nature run) of a numerical weather prediction (NWP) model without any data assimilated and use it as reference. Observations are then simulated with forward operators and the potential impact of a new observing system can be assessed by comparing NWP with or without assimilating the simulated observations. OSSEs are very expensive and challenging to run, but are much cheaper (in terms of monetary cost) than deploying a new satellite.

The forecast sensitivity to observation impacts (FSOI) method (see [Ancell and Hakim 2007](#)) uses a linearization of the data assimilation system to estimate sensitivity of NWP to all observations. FSOI is computationally cheaper to run than OSE or OSSE, but only work for a single performance metric. The linearization can either be done explicitly through

the adjoint operator like in [Baker and Daley \(2000\)](#) or implicitly through ensemble sensitivity like in [Torn and Hakim \(2008\)](#).

In fact, pioneering work by [Gandin \(1970\)](#) already had the fundamental insight of the relationship between optimal interpolation and optimal network design. Another important early work from [Huff \(1970\)](#) quantified the impact of network density reduction on precipitation areal average. The method of [Hamill and Snyder \(2002\)](#) is closely related to our approach as the only major theoretical difference is in the different statistical model for precipitation (non-Gaussian in our case). An analysis of the most important factors to consider for network design of rain gauges has been developed by [Bradley et al. \(2002\)](#) for a small case study using radar data as reference. Spatial variability of precipitation is found to be the most important factor, which further justifies our extension of stochastic precipitation model to a spatially nonstationary correlation structure. More recently, [Mauger et al. \(2013\)](#) applied ensemble sensitivity analysis for the optimal design of a climatological network for temperature and precipitation over the northwestern United States, while [Hakim et al. \(2020\)](#) applied ensemble sensitivity analysis for optimal network design from blank slate as well as from the current network in the Antarctica for analysis and 1-day forecast of surface temperature. Key differences between these previous works and our proposed method are (i) our statistical model has a component to handle intermittent and non-Gaussian precipitation events; (ii) our covariance estimates are based on the climatology derived from reanalysis, not on ensemble data assimilation; (iii) our method is applied at a larger scale on a large domain with several thousands of stations; (iv) our experiments focus on precipitation analysis, not on forecast; and (v) our method optionally takes into account the spatially and seasonally varying observation uncertainty related to wind undercatch.

The remainder of the paper is organized as follows. In the next section, the statistical model used for probabilistic QPE, the network design goal and the network design experiments are described. Experimental results follow in [section 3](#). [Section 4](#) discusses on the interpretation of the results and on the various caveats of the method. Conclusions are found in [section 5](#).

2. Data and method

a. Network design goal

It is important to define the scope of the proposed solution since an OND crucially depends on what performance metric is selected. For this study, the following assumptions are made: (i) the total life cycle cost for an individual sensor is the same for any location and sensor type; (ii) the accuracy of interpolated QPE is the only network design goal; (iii) the need for accurate precipitation measurements is uniform across the country; (iv) the fine-scale representativeness error for each sensor is uniform across the country; (v) all locations are available for the addition of new stations and all stations from the network of networks are potential candidates for removal. Of course, the reality is far more complex with (i) cost depending on both location and sensor types, (ii) multiple network design

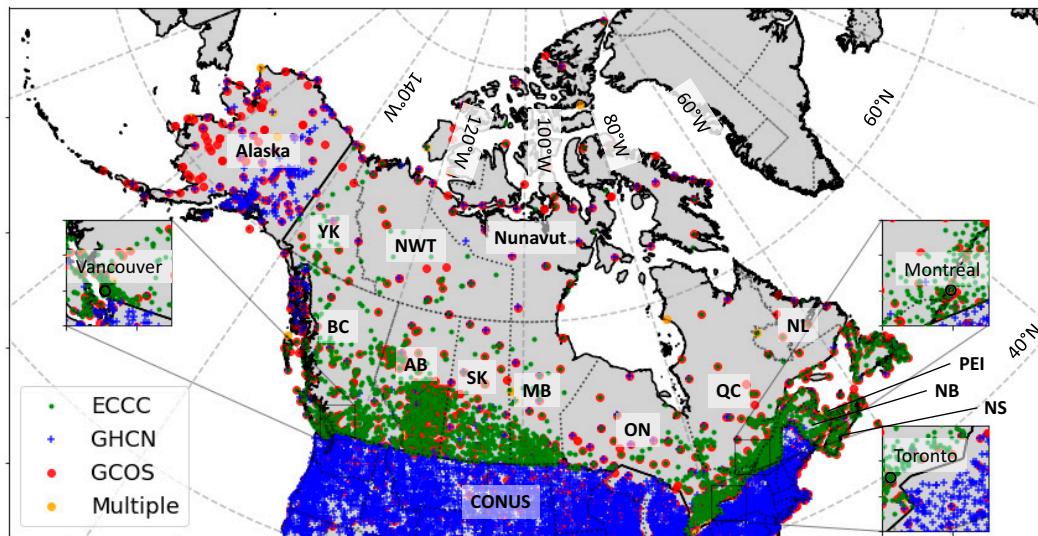


FIG. 1. Surface precipitation stations in Canada and the northern United States from several networks: Environment and Climate Change Canada (ECCC), Global Historical Climatology Network (GHCN), and Global Surface Summary of the Day (GSOD). Multiple indicates that the station is included in more than one of these networks. Provinces and territories in Canada are indicated by their initials: YK for Yukon, NWT for Northwest Territories, BC for British Columbia, AB for Alberta, SK for Saskatchewan, MB for Manitoba, ON for Ontario, QC for Quebec, NL for Newfoundland and Labrador, NB for New Brunswick, PEI for Prince Edward Island, and NS for Nova Scotia. Northern Canada suffers from many gaps in station coverage.

objectives to meet various stakeholders need, (iii) spatially variable needs with higher needs in densely populated areas, (iv) fine-scale representativeness error depending on the sensor location and the local topography, and (v) site selection depends both on the accessibility of the site and on an agreement to use a specific site. However, these simplifying assumptions provide a useful approximation of reality from which preliminary results can more easily be obtained. The proposed solution can thus be considered as useful guidance on which locations have the greatest needs for new sensors. For a truly optimal solution, these assumptions should be revisited (see section 4).

b. Data

1) STATION NETWORK

The most straightforward way to improve a precipitation analysis is to add more observational data to fill data-sparse gaps. Only considering a single network of station data will therefore be necessarily inferior to the option of integrating a “network of networks.” In Canada, and more generally in North America, there is currently no easily accessible integrated station data source combining nationally operated stations (e.g., by the Meteorological Service of Canada) with provincial/state and territory networks, including specialized networks for hydroelectric power, flood, or forest fire monitoring. The Environment and Climate Change Canada (ECCC) Climate Data Archive (Environment and Climate Change Canada 2018) does integrate provincial stations in Alberta as well as airport stations operated by Nav Canada, but more

efforts are ongoing to include more data sources. Global archive of station data such as the Global Surface Summary of the Day (GSOD) from National Centers for Environmental Information (NCEI 2018b) or the Global Historical Climatology Network daily (GHCNd) from the National Centers for Environmental Information (NCEI 2018a) do integrate many sources, but they only contain a fraction of all existing stations. Moreover, existing stations do not always report frequently depending on the length of deployment or because of maintenance issues.

The Serially Complete Dataset for North America (SCDNA) of Tang et al. (2020) provides an interim solution as it integrates daily precipitation data from ECCC stations with GSOD and GHCNd, as well as with Mexico data. SCDNA contains more than 20 000 precipitation stations reporting for at least 8 years in North America, with 2327 of these stations in Canada. A combination of various gap filling techniques has been used to ensure that the data are serially complete. We employ the station coordinates of this dataset as of 2018 as the assumed current station network. Unfortunately, station metadata (such as sensor and shielding types) are not readily available for SCDNA.

Figure 1 shows a map of the station coordinates over North America, with a close-up over subdomains around the three major metropolitan areas in Canada: Vancouver, British Columbia (BC); Toronto, Ontario; and Montreal, Quebec. Stations are color-coded by source. Only a fraction of the stations was merged from multiple sources, but for several instances, one station from ECCC was located close to a GSOD station. However, at closer inspection the time series

data appear to be distinct, indicating pairs of closely located stations. We see that at a continent scale, the contiguous United States (CONUS) is almost completely covered with stations. The only visible gaps in CONUS are over the Great Lakes, forested areas in the Maine, and some mountainous areas in western United States. However, large gaps can be seen in northern Canada and parts of Alaska. Zooming in over the Vancouver region (left inset), we see gaps mainly in mountainous regions. In the Toronto region (lower-left inset), we see gaps over large bodies of water (Lake Erie and Lake Ontario). In the Montreal region (upper-right inset), we see a lower station density as we move north. This lowering of station density away from the Canada–U.S. border is also observed all across Canada, with a higher density across the Prairie provinces (Alberta, Saskatchewan, and Manitoba) and in the Quebec City–Windsor corridor (Ontario–Quebec), but a low station density in northern Ontario and northern Quebec.

2) PRECIPITATION REANALYSIS

The enhanced land component of the fifth generation of the ECMWF reanalysis (ERA5-Land) from Muñoz-Sabater et al. (2021) is an hourly global land surface reanalysis which is downscaled from Hersbach et al.'s (2020) ERA5. The ERA5-Land dataset is selected as the reference data to build the statistical model for the proof-of-concept due to its ease of data access, its relatively high spatial resolution (0.1°), its reasonable accuracy (see, e.g., Tarek et al. 2020), its global spatial coverage over land, and its temporal coverage over more than 20 years. The total precipitation field is not assimilated directly in ERA5-Land, but it is instead interpolated from the lowest level of ERA5 (see Muñoz-Sabater et al. 2021). Precipitation observations from radar–gauge composites in the United States (Nelson et al. 2016) are assimilated in ERA5 from 2010 onward. No postprocessing adjustments are applied, but these limitations are mitigated by the improved quality of the precipitation fields in ERA5 compared to previous versions (see Hersbach et al. 2020).

Daily averaged wind speed at 10 m and temperature at 2 m from ERA5-Land are used as ancillary data for a spatially variable measurement error model and wind undercatch correction. To be consistent with a network design carried on measured precipitation records, we apply a wind undercatch correction to the ERA5-Land reanalysis data. We assume that the exact sensor and shielding type is part of epistemic uncertainty (i.e., uncertainty in not knowing the sensor metadata) and thus we lump all sensor and shield types into a wind undercatch correction function. Moreover, for cases with no or small measured precipitation amounts, a probability of precipitation is computed (see appendix D for derivation and Table D1 for parameters). Expected corrected precipitation amounts when no precipitation is measured are also derived. See appendix D for derivation details and Table D1 for fitted parameters. The correction functions are then applied daily over the whole dataset. Input data for the network design experiments are thus in the form of corrected precipitation amounts and of probability of precipitation occurrence.

Figure 2a shows a map of the expected daily total precipitation over Canada according to ERA5-Land for the 2012–21 period. There is more precipitation in the west coast and in the Canadian Rockies while there is less precipitation in the Prairies and in the north. The map of the standard deviation of daily total precipitation in Fig. 2b looks very similar. In fact, the joint scatterplot (not shown) reveals a strong correlation between the expected total daily precipitation and its standard deviation.

Figures 2c and 2d summarize temperature data into a precipitation phase index and a wind speed index, respectively. For each day, the predicted snow fraction is computed according to the following threshold: below -1°C for snow (100% snow fraction), between -1° and 3°C for mixed precipitation (50% snow fraction), and above 3°C for rain (0% snow fraction). The precipitation phase index is the average snow fraction over all days. Similarly, a wind speed index is computed by first binning wind speed into three daily average wind speed categories: low (0) for below 3 m s^{-1} , medium (1) for between 3 and 6 m s^{-1} , and high (2) for above 6 m s^{-1} . Once again, the wind speed index is the average over all the daily wind speed category values.

c. Statistical model of precipitation

1) PRIOR MARGINAL DISTRIBUTION

We consider the following statistical model for precipitation at a particular time and location. The total precipitation (water equivalent) is $X = AO$, where A is the random variable for conditional precipitation amount given a precipitation event and O is binary (i.e., Bernoulli) variable for precipitation occurrence (1 for precipitation occurrence, 0 for no precipitation). The marginal probability of the precipitation amount is assumed to follow a log-normal distribution:

$$A \sim \text{log-normal}(\mu_A, \sigma_A), \quad (1)$$

with mean μ_A and variance σ_A^2 . Other transformations have also been used in the literature such as cubic root, gamma, or Gumbel distributions in, respectively, Fortin et al. (2018), Zolina et al. (2009), and Koutsoyiannis (2004). We choose the lognormal for convenience as it allows analytical derivation of the expected variance in our statistical model. The lognormal distribution is a generally good statistical model for moderate precipitation amounts, but it is known to perform more poorly for extreme precipitation (see, e.g., Cho et al. 2004).

The probability of precipitation (PoP) occurrence is denoted by p . To later allow a smoothly spatially varying PoP, a hidden (or latent) normal distribution P with mean μ_P and variance σ_P^2 is used to generate O . A probability threshold is selected such that the probability of $P \geq 0$ is exactly the probability of precipitation p . That is, once the unobserved parameters μ_P and σ_P^2 are estimated, the sampling of precipitation occurrence is done by comparing a sample from the normal distribution with the probability threshold.

From the statistical models for O and A , we can analytically derive the expectation \mathbf{E} and variance \mathbf{V} for precipitation

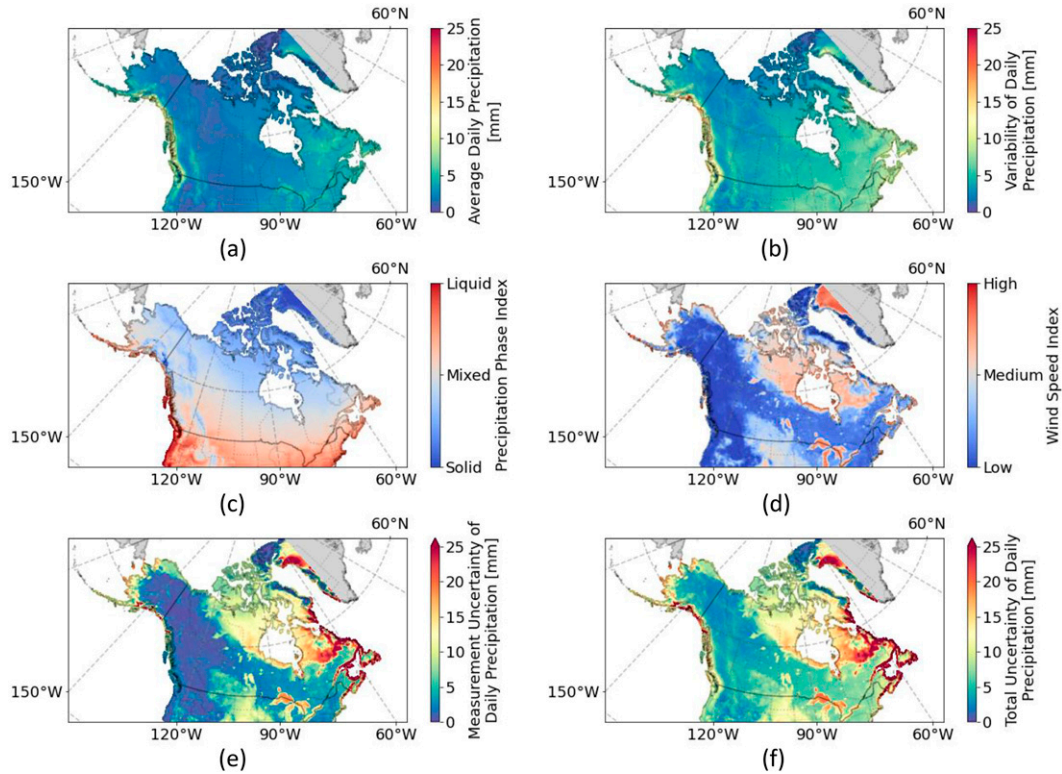


FIG. 2. Climatology from ERA5-Land for 2012–21 over all seasons over Canada and the northern United States. (a) Expected daily precipitation amount. (b) Variability (standard deviation) of daily precipitation amount. (c) Precipitation phase index. Liquid indicates predominant daily temperature average over 3°C while solid indicates predominant daily temperature average under −1°C. (d) Wind speed index. High wind indicates predominant daily wind speed average over 6 m s^{−1} while low wind indicates predominant daily wind speed average under 3 m s^{−1}. (e) Measurement uncertainty (standard deviation) of daily precipitation according to the wind undercatch error model. Note high measurement uncertainty in the East Coast, over the Great Lakes, and in Northern Quebec. (f) Total uncertainty in daily measured precipitation amount accounting for both daily precipitation variability and measurement uncertainty due to wind undercatch.

occurrence O , conditional precipitation amount A . Assuming independence between O and A , we can then derive the variance of the total precipitation X :

$$V[X] = pV[A] + p(1 - p)(E[A])^2 \quad (2)$$

(see appendix B for details). Once the parameters p , μ_A , and σ_A are estimated for a particular location, the expectation and variance of total precipitation at that location can be computed.

The method of moments is used for the initial estimation of parameters, as reproducing the expectation and the variance are more important than approximating the full distribution accurately. That is, given the sample mean and sample variance of precipitation amount, we solve for μ_A and σ_A according to the lognormal model (see appendix B). The estimated probability of precipitation occurrence \hat{p} is simply the sample frequency of precipitation events, using a threshold of $T = 0.04 \text{ mm day}^{-1}$ to discriminate between precipitation and no precipitation in ERA5-Land. This threshold is used to alleviate modeling errors for small precipitation amounts (see Hewson 2022). We use $\sigma_p^2 = \hat{p}(1 - \hat{p})$ and

$$\mu_p = -\sqrt{2}\sigma_p \text{erf}^{-1}(1 - 2\hat{p}), \quad (3)$$

where erf is the error function, to initialize the parameters of the hidden normal distribution P .

2) SPATIAL MODEL

For the spatial field of precipitation occurrence and precipitation amount, Gaussian processes are used, which is equivalent to a multivariate normal model between all observed locations and a finite number of point locations of interest. As shown in appendix A, both ensemble sensitivity techniques and optimal interpolation (or kriging) are closely related to GP as they both provide an optimal linear approximation under Gaussianity assumption.

The correlation matrices \mathbf{R}_O and \mathbf{R}_A can be estimated between pairs of locations with station observations, as well as between stations observations and potential new sensor locations. Since what follows apply for both A and O , in order to simplify the notation, we consider the general case. The covariance between locations i and j is

$$\Sigma[i, j] = \sigma[i]\mathbf{R}[i, j]\sigma[j], \quad (4)$$

where $\sigma[i]$ is the standard deviation at location i .

Let \mathbf{y} be an $N \times T$ array representing observations at N locations for T days. Let \mathbf{x} be an $M \times T$ array representing interpolated observations at M locations for T days. We denote by Σ_{xx} , Σ_{xy} , and Σ_{yy} , respectively, the covariance matrices between interpolated locations, between interpolated and observed locations, and between observed locations. Note that no particular assumptions, such as isotropic and homogeneous, are made on the correlation structure.

After applying appropriate transformations to the prior marginal distributions, the conditional probability $P(\mathbf{X} = \mathbf{x} | \mathbf{Y} = \mathbf{y})$ is assumed to follow a multivariate normal distribution with parameters $\mu_{x|y}$ and $\Sigma_{x|y}$. The update rule for these parameters according to multivariate statistics is

$$\mu_{x|y} = \mu_x + \Sigma_{xy}\Sigma_{yy}^{-1}(\mathbf{y} - \mu_y) \quad (5)$$

$$\Sigma_{x|y} = \Sigma_{xx} - \Sigma_{xy}\Sigma_{yy}^{-1}\Sigma_{xy}^T. \quad (6)$$

For fast computation of the update rule, we follow algorithm 2.1 of [Rasmussen and Williams \(2006\)](#). Since the correlation matrix Σ_{yy} is semipositive definite, it can be decomposed as $\mathbf{L}\mathbf{L}^T$ via Cholesky decomposition, where \mathbf{L} is a lower triangular matrix. Some of the computed matrices can be reused after addition of an extra station in the optimal network design experiments (see [appendix C](#) for details).

For ensemble sampling of total precipitation, the full covariance matrix Σ_{xx} is required. For a gridded field of M locations, this matrix has M^2 entries, which can become prohibitive for larger domains. A sparse version could be implemented by setting to zero any pair of location which are beyond some geographic distance. Alternatively, a coarse-to-fine multiscale approach could be investigated. For OND, since only the diagonal elements $\sigma_{x|y}^2$ of the covariance matrix $\Sigma_{x|y}$ are needed, it is not required to compute the full covariance matrix Σ_{xx} .

Covariance matrices are estimated from the climatology of ERA5-Land reanalysis with two options: 1) without considering seasonal variability, 2) by stratifying the data for warm (May–September) and cool (October–April) months. Since new observations must be simulated at locations without station data, the closest reanalysis point is used as a proxy to current and additional observations. For conditional precipitation amount, we only use samples when the pair of locations both have precipitation occurring.

3) MEASUREMENT ERROR MODEL

To account for the possibility of observational error, the exact observation covariance matrix Σ_{yy} is replaced by an observation plus error covariance matrix $\Sigma_{yy} + \Sigma_e$, where Σ_e is the observation error covariance matrix. As is often done, it is assumed that the observation error is uncorrelated, hence Σ_e is a diagonal matrix.

We consider two measurement error models: 1) a spatially homogeneous measurement error across the country for both precipitation amount and occurrence and 2) a spatially

varying measurement error for precipitation amount and occurrence, where the measurement error depends on the climatology of temperature, wind speed, and precipitation amount.

For the homogeneous error model, we take 0.05 as the logarithmic error of the precipitation amount. This measurement error corresponds approximately to an error of plus or minus 5% in measured precipitation.

For the spatially varying error model, we first estimate daily measurement errors from the fitting of residual errors in the wind undercatch correction (see [appendix D](#) and [Table D1](#) for fitted parameters). We then estimate the root-mean-square logarithmic error for precipitation amount by aggregating daily measurement errors either for warm and cool months or over the whole year.

The measurement error for the probability of precipitation occurrence is assumed to be 1% everywhere. That is, we do not attempt to quantify the uncertainty in estimating parameters for the logarithmic error of precipitation amount or for the probability of precipitation occurrence.

Given a measurement error of $\sigma_s[i]$ for a given station, we empirically choose

$$\sigma_e = \frac{1}{n} \sqrt{\sum_{i=1}^n \sigma_s^2[i]} \quad (7)$$

as the error of the areal precipitation average when n stations are available. For a homogeneous error $\sigma_s[i] \equiv \sigma_s$, the areal precipitation error will thus be $\sigma_e = \sigma_s/\sqrt{n}$. This error model assumes that all station observations within a grid cell are independent, thus reducing the variance by \sqrt{n} when averaged. In practice, we can expect a higher observation error by using more realistic assumptions than what is selected for the proof-of-concept.

The measurement errors σ_e will affect the estimation of the parameters of the lognormal precipitation amount model. Indeed, the expectation $\mathbf{E}[A_M]$ and variance $\mathbf{V}[A_M]$ of the corrected precipitation amount (i.e., after applying wind undercatch bias correction) will be inflated compared to the true expectation $\mathbf{E}[A]$ and variance $\mathbf{V}[A]$ of error-free observations. Applying the law of total expectation and the law of total variance allows to derive the expectation and variance of the error-free precipitation amounts, which can in turn be used to estimate the prior parameters μ_A and σ_A^2 for the lognormal precipitation amount model (see [appendix B](#) for derivations).

d. Network design strategy

The general principle adopted for optimal network design is to select station locations that minimize total uncertainty averaged over time. That is, representing uncertainty as the posterior variance of the probabilistic QPE, we find the location for which the sum of posterior variances over T days is the largest as the next selected location.

Network design from a blank slate allows the assessment of the potential efficiency of a network if no constraints were put on the station locations. The network efficiency for a number of stations can then be compared with the efficiency of the actual network or of proposed modifications to the network.

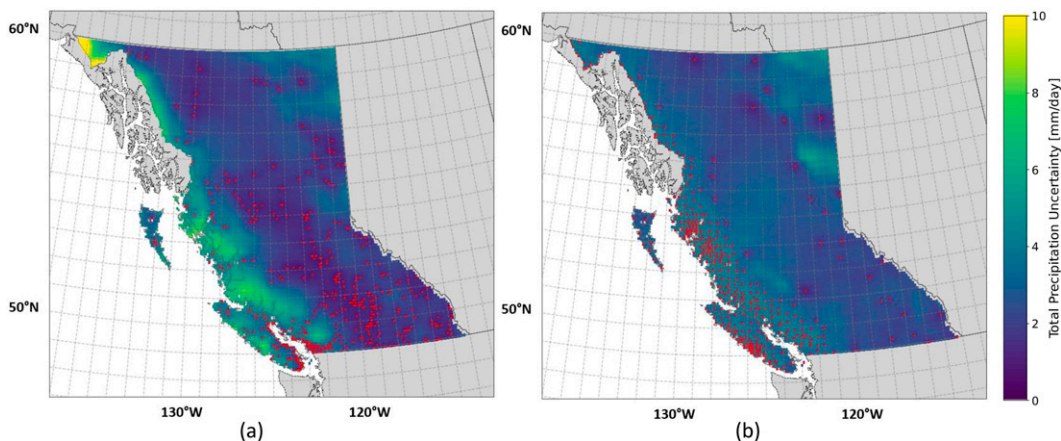


FIG. 3. Network design and uncertainty maps for the province of British Columbia for (a) current precipitation network and (b) optimal network designed from blank slate with the same number of stations as the current network.

The design strategy is to add one station at the time until the desired number of stations is reached, choosing at each step the location minimizing the total uncertainty given the previously added stations. The first station location is solely based on the prior uncertainty as derived from the statistical model.

For removing stations from a network, we would need to compute the interpolation uncertainty for all the N possible removal candidates and iterate. This strategy would require $NK - K(K - 1)/2$ updates to remove K stations. It is actually more efficient to start from a blank slate and add up to $N - K$ stations with the constraint that each added stations have to be at current station locations. If some of the K removed stations are allowed to be instead moved somewhere else, then we can start with the $N - K$ stations as before and then add back more stations without constraints on their locations.

3. Results

a. Network design experiments

We divide the Canadian domain by province and territory and perform OND experiments independently for each province and territory. This is done because computationally it is necessary to reduce the size of the domain to manage the memory required to store the covariance matrices. In addition, this division is practical since networks are often managed by provinces or territories.

1) CURRENT VS OPTIMAL NETWORK FROM BLANK SLATE

We first consider an OND experiment from a blank slate, using the statistical model with homogeneous measurement error and no seasonal stratification. The optimal location for

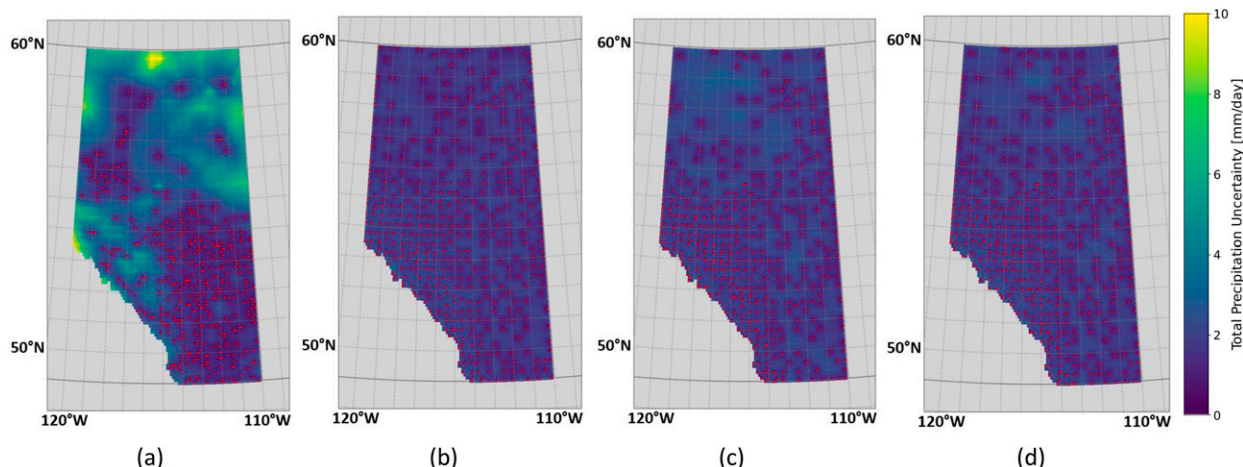


FIG. 4. Network design and uncertainty maps for the province of Alberta with uncertainty computed assuming homogeneous measurement error. (a) Current network. (b) Optimal network designed from blank slate according to homogeneous measurement error model. (c) Optimal network designed from blank slate according to spatially varying measurement error model. (d) Optimal network designed from blank slate according to spatially varying measurement error with different statistical model parameters for warm and cool months.

the first station is given by the location with maximum prior variance of the total precipitation. Stations are then added iteratively, updating the uncertainty map at each step before selecting a new location until the same number of stations as the current network is reached. Examples of resulting networks with the same number of stations than the current networks are shown in Fig. 3 for BC and Figs. 4a and 4b for Alberta.

For BC the optimal network is very dense in the coastal and mountainous region on the west of the province, and in particular for Vancouver Island, while the network has a very low density in the BC interior. This is an example where an objective method leads to counterintuitive results with a very variable network density.

For Alberta, we can see that OND is not uniformly spaced, but that a higher density of stations can be found close to the Rocky Mountains (southwest portion of the province). A lower network density is also observed in northern Alberta compared to the southeast. As expected, the resulting uncertainty map is nearly constant, with low interpolation uncertainty at all locations.

b. Network efficiency analysis

A second OND experiment is carried out for each province or territory, starting with the current network and adding up to 50 more stations within that domain.

The network uncertainty, as measured by the maximum standard deviation over the domain, is plotted against the network size (i.e., the number of stations) for several provinces and territories. This plot allows comparison between provinces and territories and to better visualize the effect of the OND method. We employ either the OND from blank slate strategy or the OND from the current network. Figure 5 shows the results in particular for two provinces: BC and Alberta.

The first striking observation that can be made from these results is how dramatic the drop of uncertainty is after adding only a few stations (i.e., two or three stations) to the current network design. Just as striking is the possibility to achieve the same interpolation uncertainty with only a small fraction of stations if the network design is started from a blank slate. For example, optimally placing 100 stations could reduce more the interpolation uncertainty than adding 50 stations to the current network design of Newfoundland and Labrador (not shown). This result indicates that the optimal course of action is neither to simply add more stations or to only remove redundant stations, but instead a redeployment of some of the stations.

The network efficiency, computed as the uncertainty of the current network over the uncertainty of the optimal network with the same number of stations, is summarized in Table 1 for all Canadian provinces and territories. The question arises as to where to add or remove stations. Given a fixed budget of 2327 stations, we assigned a number of stations in each province so that the overall interpolation uncertainty is optimally reduced when performing OND from blank slate. Table 1 summarizes the results, comparing the number of stations from the current

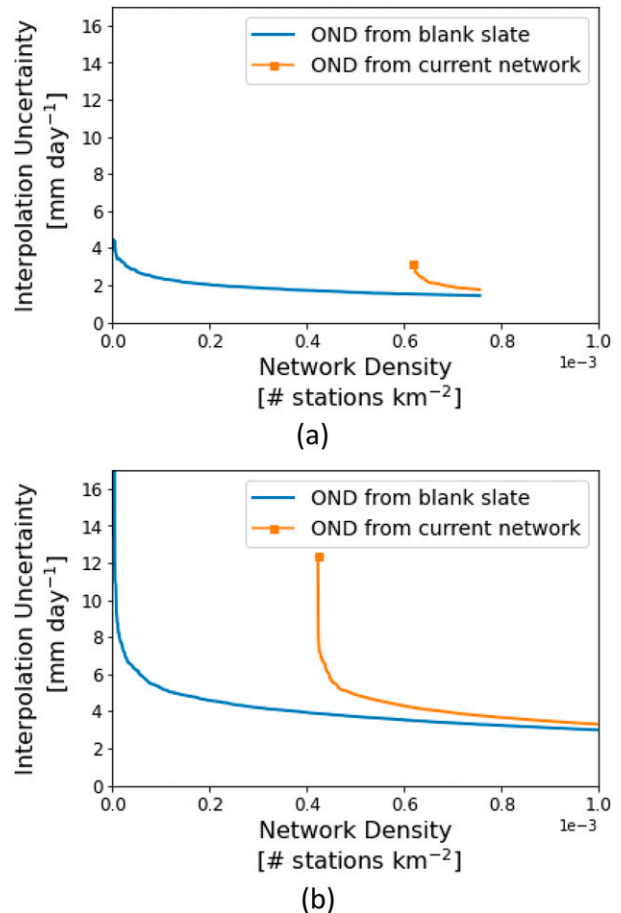


FIG. 5. Network uncertainty vs network size for stations added greedily (locally optimal) from current state or blank slate for the provinces of (a) Alberta and (b) British Columbia.

network to the number of stations for a network with an optimally allocated number of stations.

Currently, smaller Atlantic provinces have the most efficient network, with the smallest of all the provinces, Prince Edward Island (PEI), having the most efficient network. This is not very surprising given that smaller provinces tend to have more uniform networks. Yukon is the territory with the least efficient network design. Although the current network design spreads stations across the territory, it fails to properly measure precipitation in the mountainous region in the southwest. On the other hand, the optimal network design (not shown) clusters most of the stations in the mountainous region in order to reduce the uncertainty. The case is similar for BC with very different configurations between the current and the optimal network. For Newfoundland and Labrador, we can see that the network is reasonably good over Newfoundland, but a higher network density is required in Labrador in order to reduce uncertainty. Overall, we can observe that the network efficiency in Canadian provinces and territories is not very high, with only two Atlantic provinces exceeding the 50% efficiency mark.

BC is the province with the greatest need for an enhanced network, requiring 1374 stations to reduce the interpolation

TABLE 1. Current size of networks for each province and territory, as well as optimally allocated size of networks for an optimal network design from blank slate. Provinces and territories are ranked by efficiency of the current network from less (Yukon) to more (Prince Edward Island) efficient.

Province/territory	Current	Optimal	Efficiency
Yukon (YK)	38	104	5%
British Columbia (BC)	398	1374	9%
Newfoundland and Labrador (NL)	98	168	14%
Quebec (QC)	370	162	16%
Nunavut (NU)	35	53	23%
Alberta (AB)	408	52	24%
Northwest Territories (NWT)	44	35	29%
Manitoba (MB)	203	69	33%
Ontario (ON)	332	120	34%
Saskatchewan (SK)	246	42	42%
Nova Scotia (NS)	70	82	49%
New Brunswick (NB)	68	55	57%
Prince Edward Island (PEI)	17	11	83%

uncertainty to a comparable level than other provinces and territories. This is more than half of the country's assigned station budget and more than 3 times the current number of stations. Newfoundland and Labrador is another province that would require a larger network to balance the interpolation uncertainty. Other Atlantic provinces are in the middle of the pack, where a slight relative increase of stations in Nova Scotia and a slight relative decrease in the number of stations in New Brunswick would reduce overall interpolation uncertainty. The territories of Yukon and Nunavut will also benefit from enhanced networks, which is not surprising given their very sparse current network. What is surprising in fact is that they do not require as many new stations as expected given their size. Also surprising is the fact that Northwest Territories already have a more than sufficient number of stations according to the OND experiment. The two central provinces, Ontario and Quebec, could remove more than half their stations and still reach a level of interpolation uncertainty similar to what BC would attain with a network triple the size of the current network. It is even more dramatic for the Prairie provinces which would require only between 40 (Saskatchewan) and 70 (Manitoba) stations. The relatively smaller number of stations required in the Prairies can be explained by the drier climate in (part of) that region.

c. Sensitivity analysis

A sensitivity analysis was carried on by comparing the optimal network design according to the statistical model with homogeneous measurement error with the statistical model with spatially variable measurement error as well as a statistical model with parameters fitted over two seasons: warm and cool months.

The main results are presented in Fig. 4. The first observation is that there is a general agreement between the optimal network design methods (see Figs. 4b–d) to allocate a higher station density in the southwest of the province where are the Canadian Rocky Mountains, followed with a slightly lower

density in the southeast part of the province and the lowest density in the north of the province. All three variations of the method agree on the general pattern of stations and would lead to a dramatic improvement in network quality compared to the current network shown in Fig. 4a. As the uncertainty maps are shown according to the statistical model with homogeneous error model, necessarily the optimal network according to the same statistical model will perform better than any other network that are optimal according to a different criterion. This fact is confirmed by comparing the maximum total uncertainty for each network design and is seen as a lower maximum value in the uncertainty map shown in Fig. 4b. Optimal design according to a statistical model with variable error tends to concentrate even more the stations in the mountainous area at the expense of an even lower density in the north of the province. The statistical model with a spatially varying measurement error and a seasonal component is very similar to the one with no seasonality, but the concentration of stations in the mountainous area is the highest when seasonality of covariance statistics and measurement errors is considered.

For northern territories, adding the spatially variable measurement error (both with or without seasonality) leads to counterintuitive results where all the stations are clustered around the same areas in coastal or mountainous regions. For example, for Nunavut (figure not shown) the network design allocates all stations in the eastern part of the domain close to Iqaluit, while in Yukon (figure not shown) they are all allocated in the southwest part of the domain around Mount Logan. By contrast, although the optimal network design with homogeneous error model tends to allocate the majority of stations in the same areas of high precipitation variability, this latter statistical model also allocates some stations across the domain. For this reason, the statistical model with a homogeneous measurement error is preferred over the more complex statistical models with spatially varying measurement errors and seasonality.

4. Discussion

The proposed optimal network design strategy relies on specific assumptions which may or may not be valid in practice. Here, we discuss some caveats and potential extensions of the network design methodology.

The essential problem in optimal interpolation is to estimate the covariance between locations without observations. Necessarily, any approach will introduce a source of error as we can only compute the correct covariance if we already have observations at locations where we want to interpolate, but in which case we do not need to do any optimal interpolation. What is proposed in this proof-of-concept is to take reanalysis as a proxy for observations. Other alternatives would be to use radar data or do assume spatial stationarity in the covariance structure, but these alternatives would not work in Canada with a large and heterogeneous domain with only partial radar coverage. Some source of uncertainty will be introduced by the use of reanalysis, but at the same time reanalysis should be in general the best possible data we have integrating all sources of information from observations and physical knowledge. In the case of ERA5-Land, the reanalysis could

certainly be improved by integrating surface station, radar, and satellite precipitation observations to ERA5-Land. However, we quickly run into a circular argument where we need to assume a correlation structure in order to interpolate observation error, but we need the best possible analysis to estimate the correlation structure. Taking ERA5-Land directly is the simplest approach and illustrates well the concept of introducing a nonstationary correlation structure in the optimal interpolation.

The proposed network design framework can be applied for spatial and temporal scales that are no greater than the spatial scale of the underlying reanalysis data (0.1° resolution for ERA5-Land). We assumed that current and additional stations are representative at the grid scale and did not consider explicitly subgrid variability. A way to incorporate the subgrid variability would be to include an explicit subgrid model using ancillary data such as topography and land usage/cover.

Climate level monitoring, characterized by interpolation at lower temporal and spatial scales but for a longer time period, might require a very different set of assumptions for the network goals. A simple and elegant solution to satisfy both weather and climate monitoring needs would be to protect specific stations with long-term records from being moved or removed. That is, a network design could be done starting with the current climate monitoring network, gradually adding more stations to fulfill other needs.

Although the network density is very low in the north, the variability of interpolated precipitation remains generally low given the dry conditions which leads to a smaller variability in the absolute precipitation amount. On the contrary, the measurement errors are generally high as conditions above the tree line are windy and snowy, leading to large wind undercatch errors. However, adding more stations cannot reduce measurement errors and will only slightly reduce interpolation error. This issue explains the results where an optimal network design considering variable measurement errors will allocate the vast majority of stations in areas with high total precipitation uncertainty (i.e., in coastal and mountainous areas), but without significantly reducing the total uncertainty in precipitation. The solution is not intuitively satisfying, as large portions of the domain will be left with a very low network density. Even with a uniform measurement error model this phenomenon is seen, but to a lesser extent, with for example the coastal and mountainous area of BC requiring a very high network density to lower total precipitation uncertainty. Similar results can be found in [Mauger et al. \(2013\)](#) for the northwestern United States. This issue highlights the need to reduce measurement errors as much as possible with better sensors and shielding, particularly in areas of higher measurement uncertainty (yellow to red in [Fig. 2a](#)). An optimal network design considering the trade-off between installing more stations with lower cost and fewer stations with higher cost would be an important extension of this work.

Practical considerations on cost, access and land use agreement will certainly influence the final decision on the exact location of a new station, but considerations on site representativeness (not addressed here) and optimality to reduce interpolation uncertainty should be considered. In

fact, we envision the OND as providing an optimal location within a 0.1° grid cell (about 100-km^2 area). Once this area is identified, representative sites, that is locations for which the observations correlate well with the grid cell average, should be assessed given logistical constraints.

OND techniques offer flexibility in selecting optimal locations. For example, sites over water, over steep slopes, or otherwise inaccessible could be excluded when choosing the next optimal location. Similarly, if a list of candidate sites is already known, then OND can be restricted to only these potential sites. Note, however, that more constraints on potential locations will necessarily reduce the capacity of the network to effectively interpolate total precipitation.

Measurement errors have been assumed to be either constant or to depend on the climatology of temperature, wind speed, and precipitation amount, but with either the same error over the whole year or two different error models for cool and warm months. A refined OND system could instead use different observation uncertainty estimates by sensors (e.g., Pluvio, Geonor, or tipping bucket), by precipitation phase (solid, mixed, or liquid) and by environmental conditions (such as local wind and temperature) while accounting for representativeness using the local topography as predictor. However, several challenges need to be addressed before getting there. First, an up-to-date metadata repository must be collected for each current sensor. Second, a precipitation phase model (with its own uncertainty) must be included. This model will potentially require other ancillary data such as surface temperature and wind speed at sensor height, which might also need to be estimated separately with their own uncertainty (we instead assumed that the ERA5-Land provided perfect observations).

Locations where OND identified the greatest need for new stations (such as mountainous BC) are generally locations which are the most difficult to access. As such, before installing new stations, the first consideration should be if other networks not considered in the OND could be integrated in order to reduce uncertainty. OND can thus not only guide where new stations should be installed, but also help prioritize efforts to integrate other networks.

OND depends heavily on the goals of the network design. For example, the proposed network configurations demonstrated in this study minimized the maximum interpolation uncertainty over an area. A criterion to minimize the average interpolation uncertainty might lead to network which are slightly more uniform in density. If the goal is to detect precipitation events, then the uncertainty on precipitation occurrence should be minimized instead, and similarly, if we want to detect extreme precipitation events, we would minimize the uncertainty in the probability of detection of extreme events. In addition, if the relative uncertainty is minimized instead of the absolute uncertainty in total precipitation amount, then we can expect a lower network density in mountainous BC and a higher network density in the Arctic. The weighting of the network uncertainty could also be considered by putting more weight for populated areas or important infrastructures.

Sensitivity of the results to both the choice of statistical model and to the underlying data used to fit the statistical model could be further investigated. For example, if consistency in the

correlation structure coming from different data can be established (e.g., radar-derived precipitation, satellite-derived precipitation, and reanalysis), then we could further gain confidence in the results. In addition, the choice of marginal distribution to model precipitation amount as well as the way to compute the covariance structure (stationary versus spatially and/or temporally varying) could all be compared. The greedy optimization method itself could be assessed on small examples where exhaustive search is computationally feasible. A more complete evaluation of the statistical model using radar-based QPE techniques as reference is planned as future work. This evaluation will also include comparison with random or uniform network density as well as network design with isotropic and stationary correlation structure.

In summary, the assumptions made in this study could be revisited as follows:

- (i) If two or more options of sensors with different costs are considered, then the optimization procedure becomes a kind of snap-pack resource allocation problem.
- (ii) Multiple network design objectives can be optimized using a multicriteria optimization procedure. A nested strategy could be used where network design objectives at coarser resolution (e.g., for climate studies) are first answered with an allocated percentage of stations, before optimally answering needs requiring higher network density.
- (iii) Spatial variable socioeconomic needs could be considered by multiplying the interpolation uncertainty by a need index representing the relative importance of accurately measuring precipitation at each location.
- (iv) Measurements errors could be explicitly modeled by sensor and shielding type (assuming the appropriate metadata is available), whereas representativeness error could be addressed by explicitly modeling subgrid variability.
- (v) Site selection can be easily constrained to only include accessible locations. Similarly, stations from external networks or from long-term climate network can be easily protected from removal during network reduction.

5. Conclusions

A proof-of-concept of a network design methodology is demonstrated over domains covering the whole Canada. Assuming homogeneous measurement error provides reasonable results, whereas statistical models with spatially and seasonally varying measurement errors point out to the need to reduce measurement uncertainty in snowy and windy conditions.

As decisions are taken on where to add new stations or on which station to decommission, objective OND methods can offer useful guidance on the size of the network required and the locations of stations to add and remove. While the most egregious cases of redundant stations or of large gaps in the network can and should easily be dealt with subjectively, more difficult decisions on how to optimally allocate resources across the country can be informed by OND. Moreover, less obvious network design configuration can be found by the objective

method, providing quantitative recommendations for dramatic improvements in the network design quality at a minimal cost.

The optimal network design experiments reveal that the current network designs for most of the provinces and territories are rather poor. Funding to install more stations in mountainous areas, coastal areas and in the northern portions of Canadian provinces is urgently needed. The greatest needs for additional stations can be found around Mount Logan in Yukon, in the coastal areas of BC and of Newfoundland and Labrador, in northern Quebec, and in the southern portion of Baffin Island in the Everett Mountains around Iqaluit in Nunavut. The optimization of the current networks by moving or removing redundant stations could partially provide the necessary funding to install stations in harder to access locations. Indeed, small changes by adding a few stations at critical locations can have a dramatic impact in reducing interpolation uncertainty. Moreover, as optimal locations for stations within a province or territory tends to be on their boundaries, greater collaboration between provinces and territories (and between network operators in general) could provide further efficiencies.

We conclude that the proposed objective OND techniques are powerful decision-making tools for monitoring networks. The techniques developed could be readily adapted for other variables of interest such as wind speed, wind direction, maximum or minimum daily temperature or snow amount. The promises are more efficient network design at lower cost, but with better accuracy.

Acknowledgments. We would like to acknowledge engaging discussions with Guoqiang Tang and Martyn Clark from University of Saskatchewan (Canmore Coldwater Lab) in the early stage of the research. We would also like to acknowledge an internal review of the paper by Dikraa Khedhaouria (ECCC) that contributed to improve several aspects of the manuscript.

Data availability statement. Code to reproduce the experiments is available on GitLab: <https://gitlab.com/dominique.brunet/optimal-design-of-a-surface-precipitation-network-in-canada>.

APPENDIX A

Gaussian Processes, Optimal Interpolation, and Ensemble Kalman Filter

Gaussian processes are a type of stochastic process where the probability distribution of any combination of N points follow a multivariate Gaussian distribution. Optimal interpolation starts with different assumptions, but the practical implementation is exactly the same. Note that the conditional multivariate Gaussian approach is also equivalent to the Kalman update rule used in data assimilation. Indeed, if we assume that the observations are a linear function of interpolated value, i.e., $\mathbf{y} = \mathbf{H}\mathbf{x}$ where \mathbf{H} is a linear observation operator, e.g., a bilinear interpolator, then the covariance matrices can be written as $\Sigma_{yy} = \mathbf{H}\Sigma_{xx}\mathbf{H}^T$ and $\Sigma_{xy} = \Sigma_{xx}\mathbf{H}^T$. Similarly, by using the climatological averages $\boldsymbol{\mu}_x$ as background field \mathbf{x}_b (general obtained from a previous NWP run in data assimilation), we

obtain $\boldsymbol{\mu}_y = \mathbf{H}\boldsymbol{\mu}_x$ by the linear relationship between \mathbf{x} and \mathbf{y} . Renaming $\boldsymbol{\Sigma}_{xx}$ as \mathbf{P}_b and $\boldsymbol{\Sigma}_e$ as \mathbf{R} and substituting in the multivariate Gaussian update rule formula, we obtain the familiar notation for the Kalman gain

$$\mathbf{K} = \mathbf{P}_b \mathbf{H}^T (\mathbf{H} \mathbf{P}_b \mathbf{H}^T + \mathbf{R})^{-1}. \quad (\text{A1})$$

Note, however, that by directly using covariance matrices between observations and interpolated values, we can handle observations located outside the interpolated domain as well as observations that are not a linear function of the interpolated values, while avoiding the need to estimate the full covariance matrix $\boldsymbol{\Sigma}_{xx}$.

APPENDIX B

Mathematical Derivations for Marginal Distributions

a. Analytical expression for expectation and variance of total precipitation

Recall that the precipitation model is $X = OA$, where O follows a Bernoulli distribution with probability p and A follows a lognormal distribution with mean $\mathbf{E}[\log(A)] = \mu_A$ and variance $\mathbf{V}[\log(A)] = \sigma_A^2$. The expectation and variance of O are thus

$$\mathbf{E}[O] = p \quad \text{and} \quad (\text{B1})$$

$$\mathbf{V}[O] = \mathbf{E}[O](1 - \mathbf{E}[O]) = p(1 - p), \quad (\text{B2})$$

while the expectation and variance of A are

$$\mathbf{E}[A] = \exp(\mu_A + \sigma_A^2/2) \quad \text{and} \quad (\text{B3})$$

$$\mathbf{V}[A] = [\exp(\sigma_A^2) - 1] \exp(2\mu_A + \sigma_A^2). \quad (\text{B4})$$

Since we assume that O and A are independent, the expectation of X is

$$\mathbf{E}[X] = \mathbf{E}[O]\mathbf{E}[A] = p\mathbf{E}[A], \quad (\text{B5})$$

while the variance of X is

$$\begin{aligned} \mathbf{V}[X] &= \mathbf{V}[O]\mathbf{V}[A] + \mathbf{V}[O](\mathbf{E}[A])^2 + \mathbf{V}[A](\mathbf{E}[O])^2; \\ &= p(1 - p)\mathbf{V}[A] + p(1 - p)(\mathbf{E}[A])^2 + \mathbf{V}[A]p^2; \\ &= p\mathbf{V}[A] + p(1 - p)(\mathbf{E}[A])^2. \end{aligned} \quad (\text{B6})$$

The measured precipitation amount A_M (after bias correction) is assumed to have a multiplicative error so that $\log(A_M) - \log(A)$ follows a normal distribution with zero mean and variance σ_e^2 . By the law of total expectation the expectation of the reference precipitation is

$$\begin{aligned} \mathbf{E}[A_M] &= \mathbf{E}\{\mathbf{E}[A_M|A]\} \\ &= \mathbf{E}\{\exp[\log(A) + \sigma_e^2/2]\} \\ &= \exp(\sigma_e^2/2)\mathbf{E}[A] \end{aligned} \quad (\text{B7})$$

and by the law of total variance, the variance of the reference precipitation is

$$\begin{aligned} \mathbf{V}[A_M] &= \mathbf{E}\{\mathbf{V}[A_M|A]\} + \mathbf{V}\{\mathbf{E}[A_M|A]\} \\ &= \mathbf{E}\{[\exp(\sigma_e^2) - 1]\exp[2\log(A) + \sigma_e^2]\} \\ &\quad + \mathbf{V}\{\exp[\log(A) + \sigma_e^2/2]\} \\ &= [\exp(\sigma_e^2) - 1]\exp(\sigma_e^2)(\mathbf{E}[A])^2 + \exp(2\sigma_e^2)\mathbf{V}[A] \end{aligned} \quad (\text{B8})$$

To compute the variance of the measured total precipitation $X_M = O_M A_M$, we simply substitute $\mathbf{E}[A]$ by $\mathbf{E}[A_M]$ and $\mathbf{V}[A]$ by $\mathbf{V}[A_M]$ in Eq. (B6) (the estimation of the probability of precipitation p is assumed to be exact).

b. Method of moments for estimating parameters of prior distribution

Using the method of moments to solve for μ_A and σ_A^2 from $\mathbf{E}[A]$ and $\mathbf{V}[A]$, we find

$$\begin{aligned} \sigma_A^2 &= \log(\mathbf{V}[A]/\{\mathbf{E}[A]\}^2 + 1); \\ \mu_A &= \log(\mathbf{E}[A]) - \sigma_A^2/2 \end{aligned} \quad (\text{B9})$$

The mean $\mathbf{E}[A]$ and the variance $\mathbf{V}[A]$ of the reference precipitation can be derived from the mean and variance of the measured precipitation given in Eqs. (B7) and (B8). We obtain

$$\mathbf{E}[A] = \mathbf{E}[A_M]/\exp(\sigma_e^2/2) \quad \text{and} \quad (\text{B10})$$

$$\begin{aligned} \mathbf{V}[A] &= \mathbf{V}[A_M]/\exp(2\sigma_e^2) \\ &\quad - [\exp(\sigma_e^2) - 1]/\exp(2\sigma_e^2)(\mathbf{E}[A_M])^2. \end{aligned} \quad (\text{B11})$$

APPENDIX C

Implementation Details of Update Rule in Gaussian Processes

The algorithm 2.1 of Rasmussen and Williams (2006) can be rewritten as follows:

- 1) Compute Cholesky factorization $\mathbf{L}\mathbf{L}^T = \boldsymbol{\Sigma}_{yy} + \boldsymbol{\Sigma}_e$, where \mathbf{L} is a lower triangular matrix.
- 2) Solve $\mathbf{L}\mathbf{L}^T\mathbf{v} = \boldsymbol{\Sigma}_{xy}^T$.
- 3) Compute posterior mean $\boldsymbol{\mu}_{x|y} = \boldsymbol{\mu}_x + \mathbf{v}^T(\mathbf{y} - \boldsymbol{\mu}_y)$.
- 4) Compute $\boldsymbol{\alpha} = \mathbf{L}^T\mathbf{v}$.
- 5) Compute posterior variance $\sigma_{x|y}^2 = \sigma_x^2 - \boldsymbol{\alpha}^T\boldsymbol{\alpha}$.

The previously computed lower triangular matrix \mathbf{L}_N can be recuperated from the previous iteration when computing \mathbf{L} . Indeed, let \mathbf{s}_N and \mathbf{l}_N be the vectors of the first N elements of the last row of, respectively, $\boldsymbol{\Sigma}_{yy} + \boldsymbol{\Sigma}_e$ and \mathbf{L} , and let s_i and l_i be the last element of same corresponding matrices. The $(N + 1) \times (N + 1)$ matrix \mathbf{L} is thus decomposed into a $N \times N$ block \mathbf{L}_N , plus an extra row $[\mathbf{l}_N, l_i]$ and an extra column of N zeros before the last element l_i . Similarly, the $(N + 1) \times (N + 1)$ matrix $\boldsymbol{\Sigma}_{yy} + \boldsymbol{\Sigma}_e$ is decomposed into the previously computed $N \times N$ matrix with an extra row $[\mathbf{s}_N, s_i]$ and an extra column $[\mathbf{s}_N^T, s_i]$. In the Cholesky factorization of $\boldsymbol{\Sigma}_{yy} + \boldsymbol{\Sigma}_e$, the block \mathbf{L}_N will remain the same as before. What remains to be solved is

TABLE D1. Parameters for the wind undercatch uncertainty model for different precipitation phase (rain, mixed, or snow), wind speed (low, medium, or high), and measured precipitation amount (none, trace, low, or high) categories. The parameters a and b are for the bias-correcting function; the parameters α , β , and γ are for the precipitation amount measurement error; and PoP is for the probability of precipitation occurrence (see text for details). Parameters for high and low measured precipitation amount are the same, except for PoP which is always 100% for high precipitation amount (as indicated in the parentheses).

Precipitation phase	Wind speed	Precipitation amount	a	b	α	β	γ	PoP
Snow	Low	None	0.13	0			0.66	33.7
Snow	Low	Trace	0.15	0			0.47	66.1
Snow	Low	Low (high)	0.43	0.73	0.17	0.12	0.72	91.2 (100)
Snow	Medium	None	0.21	0			0.89	29.8
Snow	Medium	Trace	0.25	0			0.82	71.8
Snow	Medium	Low (high)	0.80	0.73	1.28	0.00	0.74	97.6 (100)
Snow	High	None	0.47	0			1.34	49.5
Snow	High	Trace	0.58	0			0.90	92.6
Snow	High	Low (high)	2.98	0.70	3.63	1.33	0.92	98.7 (100)
Mixed	Low	None	0.15	0			0.78	9.8
Mixed	Low	Trace	0.26	0			0.99	55.6
Mixed	Low	Low (high)	0.34	0.27	0.24	0.00	0.61	100 (100)
Mixed	Medium	None	0.47	0			0.68	11.6
Mixed	Medium	Trace	0.47	0			0.68	57.1
Mixed	Medium	Low (high)	0.47	0.53	1.47	0.00	0.68	97.8 (100)
Mixed	High	None	0.32	0			1.06	25.3
Mixed	High	Trace	0.3	0			1.29	86.7
Mixed	High	Low (high)	1.09	0.62	0.90	7.47	1.10	100 (100)
Rain	Low	None	0.11	0			0.22	1.1
Rain	Low	Trace	0.16	0			0.22	83.3
Rain	Low	Low (high)	0.10	0.21	0.00	0.04	0.40	85.7 (100)
Rain	Medium	None	0.13	0			1.34	4.9
Rain	Medium	Trace	0.20	0			0.69	46.4
Rain	Medium	Low (high)	0.00	1.00	0.01	0.43	0.80	96.2 (100)
Rain	High	None	0.12	0			0.60	4.7
Rain	High	Trace	0.11	0			0.58	41.7
Rain	High	Low (high)	0.14	0.75	0.12	0.61	0.39	90.9 (100)

- 1) the lower triangular system $\mathbf{L}_N \mathbf{I}_N^T = \mathbf{s}_N^T$ and
- 2) the last element $I_i^2 = s_i - \mathbf{I}_N \mathbf{I}_N^T$,

which can be computed efficiently.

APPENDIX D

Error Characteristic Model for Wind Undercatch

Precipitation gauges suffer from various sources of measurement errors such as capping, wetting and evaporation loss and wind undercatch (see, e.g., Mekis et al. 2018). Undercatch from solid precipitation in windy conditions is particularly severe for unshielded gauges. The catch efficiency, the ratio between measured and true precipitation falling, is generally believed to depend on wind speed, air temperature, precipitation phase and type, precipitation amount, particle size distribution, climatic conditions, sensor type, and sensor shielding. Air temperature at the gauge location can be a reasonable proxy for precipitation phase (solid, liquid, or mixed) and type (e.g., fine snowflakes or heavy and wet snow), whereas precipitation amount can provide some indication on the particle size distribution (see Colli et al. 2020).

Several attempts have been made to design universal transfer functions, that is, catch efficiency for a given wind speed and other parameters that is applicable at any location

(Kochendorfer et al. 2017, 2018, 2022; Smith et al. 2020). These transfer functions are generally designed from reference sites (or supersites) such as those in the Solid Precipitation Intercomparison Experiment (SPICE) summarized in WMO (2018). These sites use a double-fence intercomparison reference (DFAR) to estimate the true precipitation without wind undercatch and compare these reference measurements with collocated sensors which are either unshielded or with various type of wind shield. Results from these experiments cannot apply directly to provide an error characteristic for a large mixed network of daily precipitation measurements with unknown sensor and shield type.

We design daily wind undercatch bias correction and estimate the residual error after correction using Smith et al.'s (2019) quality controlled post-SPICE data from Bratt's Lake (Canada), Caribou Creek (Canada), Centre for Atmospheric Research Experiments (Canada), Marshall (United States), Haukeliseter (Norway), Formigal (Spain), Sodylanka (Finland), and Weissflyhloch (Switzerland) sites. The data are aggregated to daily measurements by accumulating precipitation and taking the daily average wind speed and temperature. Outliers for which the reference precipitation is significantly lower than the measured precipitation were removed.

Daily averaged wind is binned into low (0–3 m s⁻¹), medium (3–6 m s⁻¹), and high (6+ m s⁻¹) wind speed categories, while

precipitation phase is binned into solid/snow ($T < -1^\circ\text{C}$), mixed ($-1^\circ\text{C} \leq T < 3^\circ\text{C}$), or liquid/rain ($T \geq 3^\circ\text{C}$). The threshold for determining precipitation phase differs slightly from previous study, but they follow more closely the precipitation phase as determined by the snow fraction in ERA5-Land reanalysis.

For each of the nine binned category (i.e., the combination of wind speed and precipitation phase), a nonlinear regression is fitted between measured and reference daily precipitation with the following formula:

$$E(x) = x + ax^b, \quad (\text{D1})$$

where $a \geq 0$ and $b \leq 1$. The intuition for this regression formula is as follows. For perfect measurements, we would have $E(x) = x$, but the error from wind undercatch error is assumed to follow a power law a concave shape (since $b \leq 1$). The advantage of using this formula compared to a more complex function is that no global optimization routine is required to be called, thus mitigating the risk to fail to find a minimizer or to be stuck in a bad local minimum. The fitting procedure goes exactly as the intuition laid it out. First, the coefficients of the power law are found by linear least squares between the log of the precipitation error and the log of the measured precipitation. The coefficients a and b are then set to, respectively, 0 and 1 if outside the expected range. Second, the linear regression between the residual error after applying the power law correction and the measured precipitation is again found by least squares.

The residual error is then fitted with a linear function

$$V(x) = \alpha x + \beta, \quad (\text{D2})$$

where $\alpha, \beta \geq 0$. This error model can be interpreted as follows. The total precipitation amount (A) can be considered as the sum of N smaller precipitation amount Δ so that,

$$A = N\Delta = \sum_{i=1}^N \Delta. \quad (\text{D3})$$

The variance of the total precipitation is the sum of variance of the smaller precipitation amounts (plus a covariance term which we neglect here):

$$\text{Var}(A) = N \text{Var}(\Delta) = A \text{Var}(\Delta)/\Delta$$

with $\alpha = \text{Var}(\Delta)/\Delta$. Other measurement errors which are independent to the precipitation amount are lumped in the absolute error term (β). For small absolute errors, we thus have that the variance of precipitation is proportional to the precipitation amount, or that the standard deviation (or error) in measured daily precipitation increases as the square root of the daily precipitation amount. For extra robustness in the estimation of the parameters, we exclude the 1% greatest residual errors as outliers before estimating the parameters. For small precipitation amounts, we assume a constant logarithmic error γ which is estimated as the root-mean-square logarithmic error between reference R and corrected C precipitation

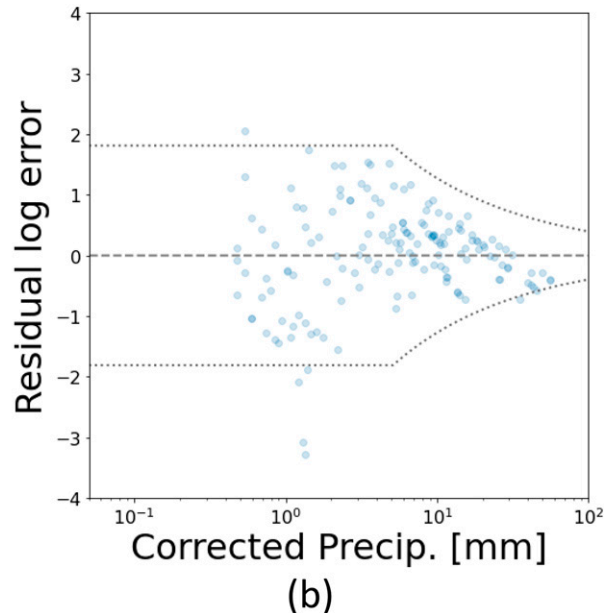
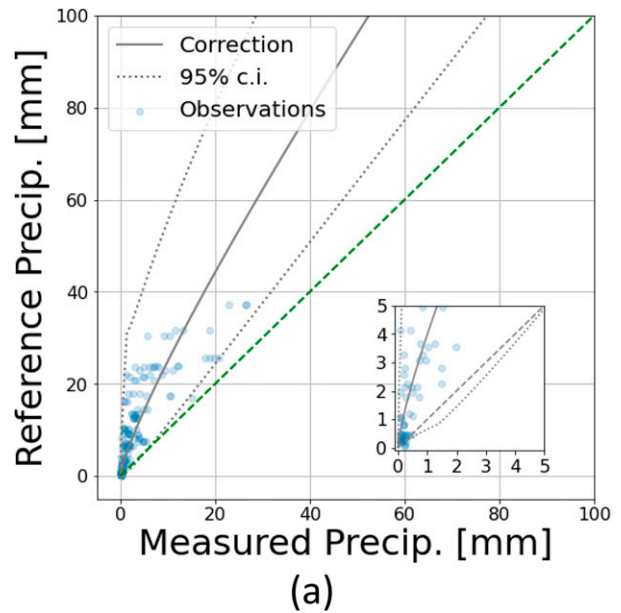


FIG. D1. Example of fit for the bias-correcting function and measurement error model for wind undercatch in the case of snow (temperature below 1°C) with high wind conditions (wind speed above 6 m s^{-1}). (a) Scatterplot of measured precipitation (for all sensors and shielding types) against reference precipitation from double fenced intercomparison gauge. The full gray line represents the wind undercatch bias correction function. The fitted 95% confidence interval is shown between the dashed lines. (b) Scatterplot of the residual logarithmic error $\log(R) - \log(C)$ against corrected precipitation amount C . The dashed lines represent the fitted 95% confidence interval according to the measurement error model.

amounts. The final measurement error model combines both errors for small and large precipitation amount:

$$R \sim \text{log-normal}[\log(C), \min(\gamma, \sqrt{\alpha C + \beta/C})]. \quad (\text{D4})$$

For our statistical model of precipitation, we also need to determine the probability of no precipitation when precipitation is measured as well as the probability of precipitation when no precipitation is measured. To do so, we simply count the number of cases for which the reference precipitation is 0 while the measured precipitation is greater than 0 and vice versa. Once again, we bin the results by wind speed and precipitation phase. Given that reference precipitation is always strictly positive when the measured daily precipitation is greater than 3 mm, we assume that the probability of precipitation is 100% in this case. If the measured daily precipitation is either none or trace (below 0.2 mm), the statistical model for precipitation amount is computed from the statistical distribution of strictly positive reference precipitation amount corresponding to these cases.

Table D1 shows the fitted parameters for wind undercatch bias correction, residual error variance and probability of precipitation for all the nine cases of wind speed and precipitation phase. An example of fitted curves and confidence intervals is shown for the snow cases with different wind speed categories in Fig. D1.

REFERENCES

- Ahnert, P., K. Hlywiak, and S. Reed, 2014: Retrospective case study of the impact of rain gage network reductions on National Weather Service river forecasts in the Susquehanna River basin. *28th Conf. on Hydrology*, Atlanta, GA, Amer. Meteor. Soc., 5.4, <https://ams.confex.com/ams/94Annual/webprogram/Paper241627.html>.
- Ancell, B., and G. J. Hakim, 2007: Comparing adjoint- and ensemble-sensitivity analysis with applications to observation targeting. *Mon. Wea. Rev.*, **135**, 4117–4134, <https://doi.org/10.1175/2007MWR1904.1>.
- Baker, N. L., and R. Daley, 2000: Observation and background adjoint sensitivity in the adaptive observation-targeting problem. *Quart. J. Roy. Meteor. Soc.*, **126**, 1431–1454, <https://doi.org/10.1002/qj.49712656511>.
- Boodoo, S., D. Hudak, A. Ryzhkov, P. Zhang, N. Donaldson, D. Sills, and J. Reid, 2015: Quantitative precipitation estimation from a C-band dual-polarized radar for the 8 July 2013 flood in Toronto, Canada. *J. Hydrometeor.*, **16**, 2027–2044, <https://doi.org/10.1175/JHM-D-15-0003.1>.
- Bradley, A. A., C. Peters-Lidard, B. R. Nelson, J. A. Smith, and C. B. Young, 2002: Raingage network design using NEXRAD precipitation estimates. *J. Amer. Water Resour. Assoc.*, **38**, 1393–1407, <https://doi.org/10.1111/j.1752-1688.2002.tb04354.x>.
- Chacon-Hurtado, J. C., L. Alfonso, and D. P. Solomatine, 2017: Rainfall and streamflow sensor network design: A review of applications, classification, and a proposed framework. *Hydrol. Earth Syst. Sci.*, **21**, 3071–3091, <https://doi.org/10.5194/hess-21-3071-2017>.
- Cho, H.-K., K. P. Bowman, and G. R. North, 2004: A comparison of gamma and lognormal distributions for characterizing satellite rain rates from the tropical rainfall measuring mission. *J. Appl. Meteor. Climatol.*, **43**, 1586–1597, <https://doi.org/10.1175/JAM2165.1>.
- Colli, M., M. Stagnaro, L. G. Lanza, R. Rasmussen, and J. M. Thériault, 2020: Adjustments for wind-induced undercatch in snowfall measurements based on precipitation intensity. *J. Hydrometeor.*, **21**, 1039–1050, <https://doi.org/10.1175/JHM-D-19-0222.1>.
- Cressie, N., 1990: The origins of kriging. *Math. Geol.*, **22**, 239–252, <https://doi.org/10.1007/BF00889887>.
- Daley, R., 1993: *Atmospheric Data Analysis*. Cambridge University Press, 472 pp.
- Environment and Climate Change Canada, 2018: Historical data. Environment and Climate Change Canada, accessed 22 December 2019, https://climate.weather.gc.ca/historical_data/search_historic_data_e.html.
- Fortin, V., G. Roy, T. Stadnyk, K. Koenig, N. Gasset, and A. Mahidjiba, 2018: Ten years of science based on the Canadian Precipitation Analysis: A CaPA system overview and literature review. *Atmos.–Ocean*, **56**, 178–196, <https://doi.org/10.1080/07055900.2018.1474728>.
- Gandin, L. S., 1965: *Objective Analysis of Meteorological Fields*. Israel Program for Scientific Translations, 242 pp.
- , 1970: The planning of meteorological station networks. WMO Tech. Note 111, WMO-265, 51 pp., https://library.wmo.int/doc_num.php?explnum_id=1800.
- Hakim, G. J., K. A. Bumbaco, R. Tardif, and J. G. Powers, 2020: Optimal network design applied to monitoring and forecasting surface temperature in Antarctica. *Mon. Wea. Rev.*, **148**, 857–873, <https://doi.org/10.1175/MWR-D-19-0103.1>.
- Hamill, T. M., and C. Snyder, 2002: Using improved background-error covariances from an ensemble Kalman filter for adaptive observations. *Mon. Wea. Rev.*, **130**, 1552–1572, [https://doi.org/10.1175/1520-0493\(2002\)130<1552:UIBEFC>2.0.CO;2](https://doi.org/10.1175/1520-0493(2002)130<1552:UIBEFC>2.0.CO;2).
- Hersbach, H., and Coauthors, 2020: The ERA5 global reanalysis. *Quart. J. Roy. Meteor. Soc.*, **146**, 1999–2049, <https://doi.org/10.1002/qj.3803>.
- Hewson, T., 2022: Known IFS forecasting issues. ECMWF Confluence Wiki, ECMWF, <https://confluence.ecmwf.int/display/FCST/Known+IFS+forecasting+issues>.
- Hoffman, R. N., and R. Atlas, 2016: Future observing system simulation experiments. *Bull. Amer. Meteor. Soc.*, **97**, 1601–1616, <https://doi.org/10.1175/BAMS-D-15-00200.1>.
- Huff, F. A., 1970: Spatial distribution of rainfall rates. *Water Resour. Res.*, **6**, 254–260, <https://doi.org/10.1029/WR006i001p0254>.
- Huffman, G. J., and Coauthors, 2019: NASA Global Precipitation Measurement (GPM) Integrated Multi-satellite Retrievals for GPM (IMERG). Algorithm Theoretical Basis Doc., version 06, 38 pp., https://gpm.nasa.gov/sites/default/files/document_files/IMERG_ATBD_V06.pdf.
- Kalinić, H., Z. Bilokapić, and F. Matić, 2021: Can local geographically restricted measurements be used to recover missing geo-spatial data? *Sensors*, **21**, 3507, <https://doi.org/10.3390/s21103507>.
- Kochendorfer, J., and Coauthors, 2017: Analysis of single-Alter-shielded and unshielded measurements of mixed and solid precipitation from WMO-SPICE. *Hydrol. Earth Syst. Sci.*, **21**, 3525–3542, <https://doi.org/10.5194/hess-21-3525-2017>.
- , and Coauthors, 2018: Testing and development of transfer functions for weighing precipitation gauges in WMO-SPICE. *Hydrol. Earth Syst. Sci.*, **22**, 1437–1452, <https://doi.org/10.5194/hess-22-1437-2018>.
- , and Coauthors, 2022: How well are we measuring snow post-SPICE? *Bull. Amer. Meteor. Soc.*, **103**, E370–E388, <https://doi.org/10.1175/BAMS-D-20-0228.1>.

- Koutsoyiannis, D., 2004: Statistics of extremes and estimation of extreme rainfall: I. Theoretical investigation/Statistiques de valeurs extrêmes et estimation de précipitations extrêmes: I. Recherche théorique. *Hydrol. Sci. J.*, **49**, 590, <https://doi.org/10.1623/hysj.49.4.575.54430>.
- Mauger, G. S., K. A. Bumbaco, G. J. Hakim, and P. W. Mote, 2013: Optimal design of a climatological network: Beyond practical considerations. *Geosci. Instrum. Methods Data Syst.*, **2**, 199–212, <https://doi.org/10.5194/gi-2-199-2013>.
- Mekis, E., N. Donaldson, J. Reid, A. Zucchini, J. Hoover, Q. Li, R. Nitu, and S. Melo, 2018: An overview of surface-based precipitation observations at Environment and Climate Change Canada. *Atmos.–Ocean*, **56**, 71–95, <https://doi.org/10.1080/07055900.2018.1433627>.
- Mishra, A. K., and P. Coulibaly, 2009: Developments in hydrometric network design: A review. *Rev. Geophys.*, **47**, RG2001, <https://doi.org/10.1029/2007RG000243>.
- Muñoz-Sabater, J., and Coauthors, 2021: ERA5-land: A state-of-the-art global reanalysis dataset for land applications. *Earth Syst. Sci. Data*, **13**, 4349–4383, <https://doi.org/10.5194/essd-2021-82>.
- NCEI, 2018a: Global Historical Climatology Network Daily (GHCNd). National Oceanic and Atmospheric Administration, accessed 18 October 2019, <http://www.ncei.noaa.gov/products/land-based-station/global-historical-climatology-network-daily>.
- , 2018b: Global Surface Summary of the Day – GSOD. National Oceanic and Atmospheric Administration, accessed 15 October 2019, <https://www.ncei.noaa.gov/access/metadata/landing-page/bin/iso?id=gov.noaa.ncdc:C00516>.
- Nelson, B. R., O. P. Prat, D.-J. Seo, and E. Habib, 2016: Assessment and implications of NCEP stage IV quantitative precipitation estimates for product intercomparisons. *Wea. Forecasting*, **31**, 371–394, <https://doi.org/10.1175/WAF-D-14-00112.1>.
- Rasmussen, C. E., and C. K. I. Williams, 2006: *Gaussian Processes for Machine Learning*. MIT Press, 266 pp.
- Seo, D.-J., 1998: Real-time estimation of rainfall fields using rain gauge data under fractional coverage conditions. *J. Hydrol.*, **208**, 25–36, [https://doi.org/10.1016/S0022-1694\(98\)00140-1](https://doi.org/10.1016/S0022-1694(98)00140-1).
- , and J. P. Breidenbach, 2002: Real-time correction of spatially nonuniform bias in radar rainfall data using rain gauge measurements. *J. Hydrometeorol.*, **3**, 93–111, [https://doi.org/10.1175/1525-7541\(2002\)003<0093:RTCOSN>2.0.CO;2](https://doi.org/10.1175/1525-7541(2002)003<0093:RTCOSN>2.0.CO;2).
- , R. Siddique, Y. Zhang, and D. Kim, 2014: Improving real-time estimation of heavy-to-extreme precipitation using rain gauge data via conditional bias-penalized optimal estimation. *J. Hydrol.*, **519**, 1824–1835, <https://doi.org/10.1016/j.jhydrol.2014.09.055>.
- , —, and P. Ahnert, 2015: Objective reduction of rain gauge network via geostatistical analysis of uncertainty in radar-gauge precipitation estimation. *J. Hydrol. Eng.*, **20**, 04014050, [https://doi.org/10.1061/\(ASCE\)HE.1943-5584.0000969](https://doi.org/10.1061/(ASCE)HE.1943-5584.0000969).
- Smith, C. D., A. Ross, J. Kochendorfer, M. E. Earle, M. Wolff, S. Buisan, Y.-A. Roulet, and T. Laine, 2019: The Post-SPICE (2015/2016 and 2016/2017) winter precipitation intercomparison data. PANGAEA, accessed 3 November 2022, <https://doi.org/10.1594/PANGAEA.907379>.
- , —, —, —, S. Buisán, Y.-A. Roulet, and T. Laine, 2020: Evaluation of the WMO Solid Precipitation Intercomparison Experiment (SPICE) transfer functions for adjusting the wind bias in solid precipitation measurements. *Hydrol. Earth Syst. Sci.*, **24**, 4025–4043, <https://doi.org/10.5194/hess-24-4025-2020>.
- Soares, J., P. A. Makar, Y. Akilu, and A. Akingunola, 2018: The use of hierarchical clustering for the design of optimized monitoring networks. *Atmos. Chem. Phys.*, **18**, 6543–6566, <https://doi.org/10.5194/acp-18-6543-2018>.
- Tang, G., M. P. Clark, A. J. Newman, A. W. Wood, S. M. Papalexiou, V. Vionnet, and P. H. Whitfield, 2020: SCDNA: A serially complete precipitation and temperature dataset for North America from 1979 to 2018. *Earth Syst. Sci. Data*, **12**, 2381–2409, <https://doi.org/10.5194/essd-12-2381-2020>.
- , —, S. M. Papalexiou, A. J. Newman, A. W. Wood, D. Brunet, and P. H. Whitfield, 2021: EMDNA: An ensemble meteorological dataset for North America. *Earth Syst. Sci. Data*, **13**, 3337–3362, <https://doi.org/10.5194/essd-13-3337-2021>.
- Tarek, M., F. P. Brissette, and R. Arsenault, 2020: Evaluation of the ERA5 reanalysis as a potential reference dataset for hydrological modelling over North America. *Hydrol. Earth Syst. Sci.*, **24**, 2527–2544, <https://doi.org/10.5194/hess-24-2527-2020>.
- Torn, R. D., and G. J. Hakim, 2008: Ensemble-based sensitivity analysis. *Mon. Wea. Rev.*, **136**, 663–677, <https://doi.org/10.1175/2007MWR2132.1>.
- WMO, 2018: WMO Solid Precipitation Intercomparison Experiment (SPICE) (2012–2015). IOM Rep. 131, WMO, 1445 pp., https://library.wmo.int/doc_num.php?explnum_id=5686.
- Zhang, J., and Coauthors, 2016: Multi-Radar Multi-Sensor (MRMS) quantitative precipitation estimation: Initial operating capabilities. *Bull. Amer. Meteor. Soc.*, **97**, 621–638, <https://doi.org/10.1175/BAMS-D-14-00174.1>.
- Zolina, O., C. Simmer, K. Belyaev, A. Kapala, and S. Gulev, 2009: Improving estimates of heavy and extreme precipitation using daily records from European rain gauges. *J. Hydrometeorol.*, **10**, 701–716, <https://doi.org/10.1175/2008JHM1055.1>.